# Medium Access Probability Model Based on CSMA/CA for a DSRC Network Driven by Poisson Line Process

Abdel Karim Ajami, Hassan A. Artail, Karim Y. Kabalan
Electrical and Computer Engineering Department, American University of Beirut, Beirut, Lebanon
E-mails: {aa377, hartail, kabalan}@aub.edu.lb

***Abstract*—Vehicular networks are gaining a huge momentum as a mean for an intelligent transportation system that can address numerous problems related to traffic monitoring, accidents, autonomous driving, etc. However, the deployment of vehicular networks is a big challenge for vehicles manufacturers and governments in terms of responsibility and cost. Compared to related research efforts that assume a fixed medium access probability (MAP) of nodes, this paper presents an analytical model using the stochastic geometry tool where we derive the MAP of DSRC nodes in a network composed of vehicles (DSRC nodes) that are located on a system of roads. We then model the roads using a Poisson line process (PLP) and the locations of nodes on each road as a homogeneous 1D Poisson point process (PPP). Also, we model the MAP based on the IEEE 802.11p standard, where we consider the effect of interference and the carrier sense multiple access with collision avoidance (CSMA/CA). We validated the analytical model against Monte Carlo simulations to prove its accuracy and reliability. The importance of our work stems from the fact that the developed MAP model contributes to the understanding of future DSRC network deployments.**

***Index Terms*—Medium Access Probability; Stochastic Geometry; Poisson Line Process; DSRC;**

## I. Introduction and Related Work

In the recent years, traffic congestion and accidents have become important global issues. The World Health Organization (WHO) reported that every year more than 100 million people die in traffic accidents worldwide resulting in economic losses of up to $500 billion [2]. Hence, there is a room to significantly enhance the safety and efficiency of current transportation systems using intelligent transportation systems (ITS) [1]. ITS are expected to address issues related to traffic monitoring, accidents, road congestion, autonomous driving, etc. As they are an enabler for ITS, vehicular networks have been gaining a considerable interest, and are in effect designed to support information exchange using Vehicle-to-Vehicle (V2V) and Vehicle-to-Infrastructure (V2I) communications.

A vehicular network contains vehicles as well as road side units (RSUs) which are computing devices that are deployed on the side of the road to exchange safety-related messages with vehicles. The V2V and V2I communications are enabled by the IEEE 802.11p protocol which is an amendment to the IEEE 802.11 standard that defines the physical (PHY) and medium access control (MAC) layer specifications [3]. In 1999, the 5.850-5.925 GHz spectrum ITS band was allocated by the Federal Communication Commission (FCC) to vehicular communications. This band is referred to as dedicated short range communications (DSRC).

Recently, a growing interest has been witnessed in modeling vehicular networks using the stochastic geometry mathematical tool [6]–[8], which was proven to be highly effective in analyzing the performance of wireless networks and their random spatial patterns [9]–[11], [13]. Stochastic geometry provides a systematic approach for understanding the trends in deploying vehicular networks, which is the biggest challenge, as reported by the Michigan Department of transportation (MDoT) and the Center for Automotive Research (CAR) [14]. In this regard, the authors in [15] investigated the best spatial modeling for vehicular networks, where they analyzed the probability mass functions of datasets obtained from the mobile taxi trajectory records in several cities. The authors showed that the Cox process model can provide the best characterization of the spatial point patterns of random vehicle locations in these cities. In addition, the use of Poisson line process (PLP) based Cox point process was investigated in [16], where several statistical properties were derived, such as the nearest neighbor distribution. Moreover, in [17], the coexistence of DSRC (the 802.11p standard governing V2V and V2I communications) and Wi-Fi based on the proposal of the FCC was studied, although a 2D homogenous PPP model was employed to simplify the analysis. On the other hand, a more applicable Cox point process model was presented in [18] to model the vehicular communication system, and it was compared with the standard 2D homogenous PPP model, where the results showed that the Cox point process model is more accurate in particular node density scenarios. However, so far, analytical models based on the Cox point process have all assumed a fixed medium access probability (MAP) with a PLP, and therefore they do not allow for modeling the effect of the carrier sense multiple access with collision avoidance (CSMA/CA) based on the IEEE 802.11p standard.

In this paper, we address this issue and present an analytical model for the MAP of DSRC nodes in a vehicular network

composed of wireless nodes that are located on a system of roads. We model the roads using a PLP and the locations of nodes on each road as a homogeneous 1D Poisson point process (PPP). The contributions of the paper are as follows:

- Developing a PLP-based framework that models the MAP of DSRC nodes based on the IEEE 802.11p standard.
- Considering the effect of interference and the CSMA/CA channel access mechanism using a modified Matern hard-core point process instead of using a fixed MAP, while also accounting for different traffic types.
- Validating the new MAP model against Monte Carlo simulations.
- Presenting an analysis that considers voice (high priority) and background (low priority) traffic to illustrate the impact of DSRC node and road densities on the MAP of nodes. This helps to understand the performance of high priority traffic such as critical safety messages transmitted on the control channel (CCH) of DRSC.

## II. System Model

In this section, we describe the spatial and radio channel model, as well as the channel access model for the DSRC network under study.

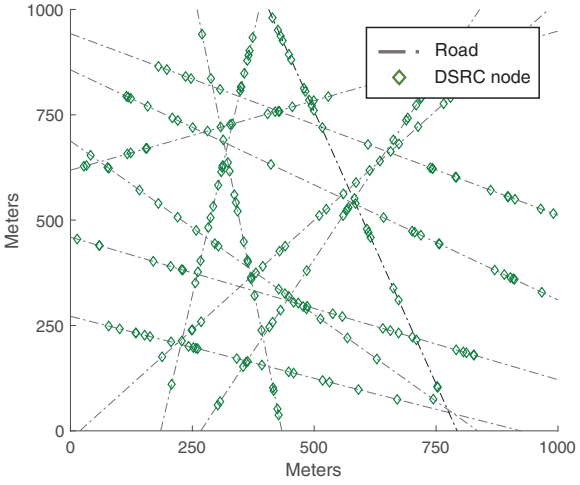


Fig. 1: DSRC Network

### A. Spatial and Radio Channel Model

We consider a DSRC network that consists of DSRC nodes (RSUs and vehicles) that communicate on a typical geographical area containing roads as shown in Figure 1. We model the road locations as a stationary motion-invariant Poisson line process (PLP) $\Phi_R$ [18] with a line density $\rho_l$. The line density $\rho$ is defined as the mean line length per unit area. The density of the corresponding point process in the representation space $[0, 2\pi] \times [0, \infty]$ is given by $\lambda_l = \frac{\rho_l}{2\pi}$. Consistent with [18], each line in a PLP is defined using two parameters. The first parameter is the distance $y_n \in [0, \infty]$ for $n = \{1, 2, 3, ...\}$, which represents the $n^{th}$ nearest perpendicular projection distance from the origin o to each line $L_n$. The second parameter is the angle $\theta \in (0, 2\pi]$ between the x-axis and $y_n$ and is measured in a counter clockwise direction. For mathematical tractability, we consider a motion-invariant PLP where $\theta$ is uniformly distributed in $(0, 2\pi]$. We then model the locations of wireless DSRC nodes, which include vehicular nodes and RSUs, on each line (road) using a homogenous 1D PPP with density $\lambda_v$. We assume that the DSRC nodes have full buffer traffic and that all nodes will contend to access the channel using CSMA/CA based on the IEEE 802.11p protocol, as described in the next subsection. The signal path loss between a DSRC node located at $\zeta_n$ and another DSRC node located at $\zeta_m$ is modeled as $\ell(||\zeta_n - \zeta_m||) = \frac{c}{4\pi f_c}\|\zeta_n - \zeta_m\|^\alpha$ with $f_c$ standing for the carrier frequency, $c$ for the speed of light, and $\alpha$ for the path loss exponent. We consider an outdoor path loss model with $\alpha$ = 4 [19].

We assume that channels are subject to Rayleigh fading, such that the power fading coefficient $G_{d_i d_j}^{D_i D_j}$ between the transmitting and receiving DSRC nodes is exponentially distributed with parameter $\beta$. Based on Slivnyak's theorem [6], we can equivalently focus our study on the performance of a typical DSRC node assumed to be located in the origin.

### B. Channel Access

The IEEE 802.11p amendment defines the MAC and PHY layer protocols used by DSRC nodes. These protocols are part of the Wireless Access in Vehicular Environments (WAVE) standard that also includes the set of IEEE 1609.x protocols enabling upper layer operational aspects across the multiple channels of DSRC. The DSRC bandwidth is divided into seven channels including six service channels (SCHs) and one control channel CCH, with the latter being allocated mainly for communicating road safety messages, as shown in Figure 2. Vehicles having a single radio use time division to operate on the CCH and SCHs. The multi-channel operations are defined in the upper MAC layer of the IEEE 1609.4 protocol, and use time division to switch between the CCH channel and one of the six SCH channels by spending 50ms in each.

In the 802.11p protocol, there is no feedback mechanism provided by the receiver, and hence, the contention window size of the 802.11p transmitter remains fixed. Moreover the IEEE 802.11p protocol employs the EDCA mechanism for contention-based prioritized QoS support. According to EDCA, a station (node) can implement up to four access categories (ACs) with different priorities corresponding to background traffic (AC 0), best effort (AC 1), video (AC 2), and voice (AC 3) [5]. Each AC can be identified by a different set of channel access parameters, including the contention window size (CW), the Arbitrary Inter-Frame Spacing (AIFS), and the AIFS Number (AIFSN[AC]). When using the CSMA/CA protocol, a DSRC node performs the clear channel assessment (CCA) procedure to detect the presence of active transmitters for which the received signal power surpasses a

given detection threshold. A channel is determined busy if the transmitter discovers another DSRC signal that exceeds the carrier sense (CS) threshold $\Gamma_{cs}$. If the channel is found idle, the DSRC node will implement prior to transmission a back-off period, which gets randomly selected from the contention window CW. This window is a set of possible values that depend on the traffic type and the corresponding AC, in order to determine the priority of the DSRC node for accessing the medium.

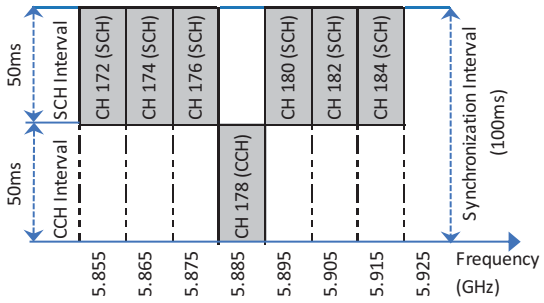


Fig. 2: DSRC Channel Allocation

We define the contender of a DSRC node $\zeta_{d_i}$ that belongs to a 1D PPP $\Phi_{D_i}$ of a particular road as other DSRC nodes that belong to the same road $\Phi_{D_i}$ or a different road $\Phi_{D_{j\neq i}}$ from which the received power at $\zeta_{d_i}$ exceeds the threshold $\Gamma_{cs}$. Each DSRC node $\zeta_{d_i}$ has a random back-off variable $t_{d_i}^{D_i}$ that is uniformly distributed in the interval $[\Delta, \Delta + CW - 1]$. We consider mainly two types of traffic which are voice (high priority) and background traffic (low priority). As for voice traffic, $t_{d_i}^{D_i}$ is uniformly distributed in the interval $[0, 7]$ whereas in case of background traffic, $t_{d_i}^{D_i}$ is uniformly distributed in the interval $[5, 1028]$. Notice that we apply an offset to the background traffic contention window size $[0, 1023]$ in order to model the difference between the inter-frame spacing of voice and background traffic [5]. Each DSRC node will be retained when contending for channel access if it has a smaller back-off period (timer) than all of its contenders. A medium access indicator $e_{d_i}^{D_i}$ is therefore assigned to each DSRC node, which is equal to one if the node is allowed to transmit by the corresponding MAC layer protocol, and zero otherwise.

## III. Medium Access Probabilty

In this section we derive the medium access probability of a DSRC node that belongs to a Cox process based on a PLP. When DSRC nodes (vehicles and RSUs) co-exist with each other in the same band, each node will contend using the EDCA mechanism to access the channel. Given that each node may belong to a particular line (road), we consider the probability that a node may contend with another node located on the same line or with nodes that belong to a different line. Thus, we derive the medium access indicator $e_{d_0'}^{D_0}$ of a DSRC node $\zeta_{d_0'} \in \Phi_{D_0}$ where $\Phi_{D_0}$ corresponds to the 1D PPP of the DSRC nodes that belong to the same line, and $\Phi_{D_n} \forall\ n = 1 \ldots N$ corresponds to the 1D PPP of the nodes that belong to the $n^{th}$ nearest line (where $N$ tends to $\infty$):

$$e_{d_0'}^{D_0} = \prod_{\zeta_{d_0}\in\Phi_{D_0}\setminus\{\zeta_{d_0'}\}} \left(\mathbb{1}_{t_{d_0}^{D_0}\geq t_{d_0'}^{D_0}} + \mathbb{1}_{t_{d_0}^{D_0}<t_{d_0'}^{D_0}} \mathbb{1}_{G_{d_0d_0'}^{D_1}/l\left(\|\zeta_{d_0}-\zeta_{d_0'}\|\right)\leq \Gamma_{cs}/P_D}\right)$$
$$\times \prod_{\zeta_{d_1}\in\Phi_{D_1}} \left(\mathbb{1}_{t_{d_1}^{D_1}\geq t_{d_0'}^{D_0}} + \mathbb{1}_{t_{d_1}^{D_1}<t_{d_0'}^{D_0}} \mathbb{1}_{G_{d_1d_0'}^{D_1D_0}/l\left(\|\zeta_{d_1}-\zeta_{d_0'}\|\right)\leq \Gamma_{cs}/P_D}\right)$$
$$\vdots$$
$$\times \prod_{\zeta_{d_N}\in\Phi_{D_N}} \left(\mathbb{1}_{t_{d_n}^{D_N}\geq t_{d_0'}^{D_N}} + \mathbb{1}_{t_{d_n}^{D_N}<t_{d_0'}^{D_0}} \mathbb{1}_{G_{d_nd_0'}^{D_ND_0}/l\left(\|\zeta_{d_n}-\zeta_{d_0'}\|\right)\leq \Gamma_{cs}/P_D}\right) \quad (1)$$

Note that $\mathbb{1}_A$ is the indicator function of the event $A$, which is equal to one if $A$ exists and zero otherwise. Equation (1) indicates that if a DSRC node does not sense the transmission of any other node, or it senses the transmission of another node while it has the smallest random backoff (timer), whether that node is on the same road or on a different one, it will get access to the channel, and its medium access indicator will be set to 1.

***Lemma 1:*** When the DSRC nodes of a single DSRC network adopt the contention window $[\Delta, \Delta + CW - 1]$, the MAP of a DSRC node that belongs to a Cox process based on a PLP is derived in (2).

*Proof:* Given the tagged DSRC node we have:

$$\mathbb{E}\left[e_{d_0'}^{D_0} | t_{d_0'}^{D_0} = t, \zeta_{d_0'} = (r_0, 0), \zeta_{d_0'} \in \Phi_{D_0}\right]$$
$$= \mathbb{E}\Bigg[\prod_{\zeta_{d_0}\in\Phi_{D_0}\setminus\{\zeta_{d_0'}\}} \left(\mathbb{1}_{t_{d_0}^{D_0}\geq t_{d_0'}^{D_0}} + \mathbb{1}_{t_{d_0}^{D_0}<t_{d_0'}^{D_0}} \mathbb{1}_{G_{d_0d_0'}^{D_1}/l\left(\|\zeta_{d_0}-\zeta_{d_0'}\|\right)\leq \Gamma_{cs}/P_D}\right)$$
$$\times \prod_{\zeta_{d_1}\in\Phi_{D_1}} \left(\mathbb{1}_{t_{d_1}^{D_1}\geq t_{d_0'}^{D_0}} + \mathbb{1}_{t_{d_1}^{D_1}<t_{d_0'}^{D_0}} \mathbb{1}_{G_{d_1d_0'}^{D_1D_0}/l\left(\|\zeta_{d_1}-\zeta_{d_0'}\|\right)\leq \Gamma_{cs}/P_D}\right)$$
$$\vdots$$
$$\times \prod_{\zeta_{d_N}\in\Phi_{D_N}} \left(\mathbb{1}_{t_{d_n}^{D_N}\geq t_{d_0'}^{D_N}} + \mathbb{1}_{t_{d_n}^{D_N}<t_{d_0'}^{D_0}} \mathbb{1}_{G_{d_nd_0'}^{D_ND_0}/l\left(\|\zeta_{d_n}-\zeta_{d_0'}\|\right)\leq \Gamma_{cs}/P_D}\right)\Bigg]$$
$$\overset{(a)}{=} \mathbb{E}\left[\prod_{\zeta_{d_0}\in\Phi_{D_0}\cap B^c(0,r_0)} \left(1 - F_{CW}(t)\exp\left(-\mu\frac{\Gamma_{cs}}{P_D} l\left(\|\zeta_{d_0} - \zeta_{d_0'}\|\right)\right)\right)\right]$$
$$\times \mathbb{E}\left[\prod_{\zeta_{d_1}\in\Phi_{D_1}} \left(1 - F_{CW}(t)\exp\left(-\mu\frac{\Gamma_{cs}}{P_D} l\left(\|\zeta_{d_1} - \zeta_{d_0'}\|\right)\right)\right)\right]$$

$$\mathbb{P}_{\text{MAP}} = \int_0^\infty \int_0^{CW} \exp\Bigg[ - F_{CW}(t)\lambda'_{D_0} \int_{\mathbb{R}^2\setminus B(0,r)} \exp\left(-\mu\frac{\Gamma_{cs}}{P_D} l\left(\|\zeta_{d_0} - \zeta_{d_0'}\|\right)\right) - F_{CW}(t) \sum_{n=1}^{\infty} \lambda'_{D_n} \int_{\mathbb{R}^2} \exp\left(-\mu\frac{\Gamma_{cs}}{P_D} l\left(\|\zeta_{d_n} - \zeta_{d_0'}\|\right)\right)\Bigg] f_R(r_0)\mathrm{d}t\mathrm{d}r_0 \quad (2)$$

$$\times \mathbb{E}\left[\prod_{\zeta_{d_N}\in\Phi_{D_N}}\left(1-F_{CW}(t)\exp\left(-\mu\frac{\Gamma_{cs}}{P_D}l\left(\|\zeta_{d_N}-\zeta_{d_0'}\|\right)\right)\right)\right]$$

$$\overset{(b)}{=}\exp\Bigg[-F_{CW}(t)\lambda'_{D_1}\int_{\mathbb{R}^2\setminus B(0,r)}\exp\left(-\mu\frac{\Gamma_{cs}}{P_D}l\left(\|\zeta_{d_0}-\zeta_{d_0'}\|\right)\right)$$
$$-F_{CW}(t)\lambda'_{D_2}\int_{\mathbb{R}^2}\exp\left(-\mu\frac{\Gamma_{cs}}{P_D}l\left(\|\zeta_{d_1}-\zeta_{d_0'}\|\right)\right)$$
$$\vdots$$
$$-F_{CW}(t)\lambda'_{D_N}\int_{\mathbb{R}^2}\exp\left(-\mu\frac{\Gamma_{cs}}{P_D}l\left(\|\zeta_{d_N}-\zeta_{d_0'}\|\right)\right)\Bigg] \tag{3}$$

where (a) follows by re-writing $\zeta_{d_0'}=(r_0,0)$ as $\zeta_{d_0'}\in\Phi_{D_0}$, $\Phi_{D_0}(B^o(0,r_0))=0$, de-conditioning on $\Phi_{D_0}(B^o(0,r_0))=0$, and from the independence of $\Phi_{D_0}$ and $\Phi_{D_{j\geq 1}}$. By using Slivnyak′s theorem, and the probability generating functional (P.G.FL) of the PPP, (b) is derived, where $N$ tends to $\infty$. $\lambda'_{D_n}$ is the equivalent line density of the 1D PPP in $\mathbb{R}^2$. $\lambda'_{D_n}$ can be derived by using the probability of a node to exist on a particular line (e.g. same or nearest $n^{th}$ line). Thus $\lambda'_{D_n}=\mathbb{P}[\varepsilon_n]\times\rho_l\times\lambda_v$ where $\mathbb{P}[\varepsilon_n]$ is the probability of event $\varepsilon_n$ that is derived in [18]. $\varepsilon_0$ corresponds to the event that $\zeta_0^{D_1}$ falls on the same road as the typical DSRC node, whereas $\varepsilon_n$ corresponds to the event that $\zeta_0^{D_1}$ falls on the $n^{th}$ nearest road to the typical DSRC node, with $n=1,2,3,...,\infty$. $\mathbb{P}[\varepsilon_0]$ is the probability of the event $\varepsilon_0$ and is defined as:

$$\mathbb{P}[\varepsilon_0]=\int_0^\infty\left(1-\exp\left(-2\lambda_v v_0\right)\right)\left(2\pi\lambda_l\int_0^{v_0}f_{T_n}(v_0|z)\,dz\right)$$
$$\times\exp\left(-2\pi\lambda_l\int_0^{v_0}F_{T_n}(v_0|z)\,dz\right)dv_0 \tag{4}$$

Where $F_{T_n}(t_n|y_n)=1-\exp\left(-2\lambda_v\sqrt{t_n^2-y_n^2}\right)$ and $f_{T_n}(t_n|y_n)=\frac{2\lambda_v t_n}{\sqrt{t_n^2-y_n^2}}\exp\left(-2\lambda_v\sqrt{t_n^2-y_n^2}\right)$. Note that $F_{T_n}(.)$ and $f_{T_n}(.)$ are respectively the Cumulative Density Function (CDF) and the PDF of the distance between the typical DSRC node and the closest DSRC node that is found on the $n^{th}$ nearest road. On the other hand, $\mathbb{P}[\varepsilon_n]$ is the probability of event $\varepsilon_n\,\forall\, n>0$ defined as:

$$\mathbb{P}[\varepsilon_n]=\int_0^\infty\mathbb{P}[\varepsilon_n|Y_n]\,f_{Y_n}(y_n)d_{t_n} \tag{5}$$

Where $\mathbb{P}[\varepsilon_n|Y_n]$ is the probability of the event $\varepsilon_n$ conditioned on the perpendicular projection $y_n$:

$$\mathbb{P}[\varepsilon_n|Y_n]=\int_0^\infty\exp\left(-2\lambda_v t_n\right)\left(1-F_{U_n}(t_n|y_n)\right)$$
$$\times\left(1-F_{V_n}(t_n|y_n)\right)f_{T_n}(t_n|y_n)\,d_{t_n} \tag{6}$$

Where $F_{U_n}(t_n|y_n)$ and $F_{V_n}(t_n|y_n)$ are defined in eqs. (8) and (9), respectively. Finally, $f_{Y_n}(y_n)$ in eq. (5) is the PDF of the distance $y_n$:

$$f_{Y_n}(y_n)=\exp\left(-2\pi\lambda_l y_n\right)\frac{\left(2\pi\lambda_l y_n\right)^n}{y_n\,(n-1)!} \tag{7}$$

Then by de-conditioning on $t$ with $F_{CW}(t)=\frac{t-\Delta}{CW-\Delta}$ and on $||\zeta_{d_0'}||$ we get the resulting MAP equation in (2). ■

## IV. Performance Evaluation

In this section, we present Monte Carlo simulation results from a spatial discrete event simulator to assess the accuracy of the analytical MAP model. The simulation parameters considered are shown in Table I. We consider high and low road density, and consistent with the literature [17], we set the power fading parameter to $\beta=1$.

TABLE I: Simulation Parameters

| **Parameter** | **Value** | **Parameter** | **Value** |
|---|---|---|---|
| $P_D$ | 20 dBm | $\Gamma_{cs}$ | $-82$ dBm |
| $f_c$ | 5.9 GHz; | $c$ | $3\times10^8 m/s$ |
| $\alpha$ | 4 | $\beta$ | 1 |
| Radius | 1 km | $CW$ | 7 |

We start first by analyzing $\mathbb{P}[\varepsilon_n]$, which is the probability of any DSRC node to be located on the same line of the typical node or on the $n^{th}$ closest line. Evaluating this probability is important from the point of view of studying the impact on the ability of the DSRC node to access the medium, and then to transmit its data. Figure 3 shows $\mathbb{P}[\varepsilon_n]$ from $n=0$ till $n=7$ for different DSRC node densities in case of voice traffic.

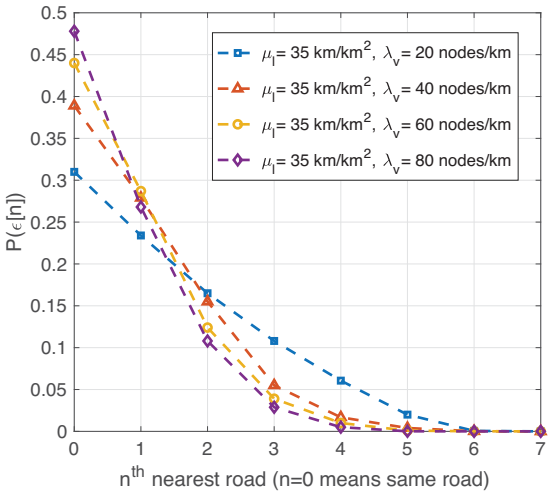


Fig. 3: Probability for a DSRC node to be located on the same or the nearest $n^{th}$ line

From Figure 3, we can see that when there are 40 or more vehicles per Kilometer of a road segment (i.e., $\lambda_v\geq 40$), the MAP of a DSRC node will mainly be affected by nodes on up to 4 roads away (i.e., nearest 4 roads), and of course including nodes on the same road. However, when $\lambda_v\leq 40$, nodes on up to the 6 nearest roads could affect the MAP of the typical node. Next, we shed more light on analyzing the MAP of a DSRC node with respect to the variation of the node density as

$$F_{U_n}\left(u_n|y_n\right)=\begin{cases}1-\left(1-\frac{u_n}{y_n}+\frac{1}{y_n}\int_0^{u_n}\left(1-F_{T_n}\left(u_n|z\right)\right)dz\right)^{n-1} & \text{if } 0\leq u_n<y_n\\ 1-\left(\frac{1}{y_n}\int_0^{y_n}\left(1-F_{T_n}\left(u_n|z\right)\right)dz\right)^{n-1} & \text{if } y_n\leq u_n<\infty\end{cases} \tag{8}$$

$$F_{V_n}\left(v_n|y_n\right)=1-\exp\left(-2\pi\lambda_l\int_{y_n}^{v_n}F_{T_n}\left(v_n|z\right)dz\right),\text{if } y_n\leq v_n<\infty \tag{9}$$

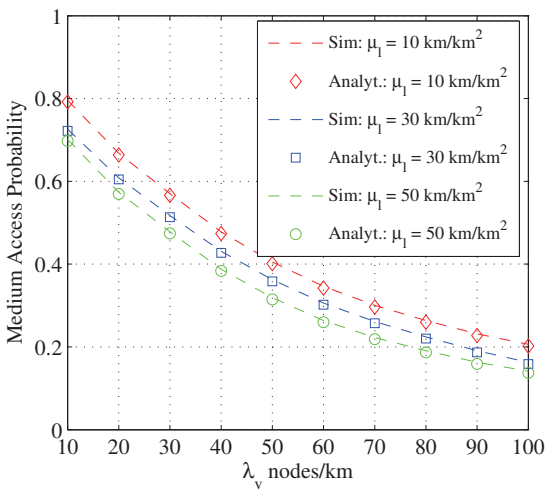


Fig. 4: Medium access probability (MAP) versus DSRC node density $\lambda_v$

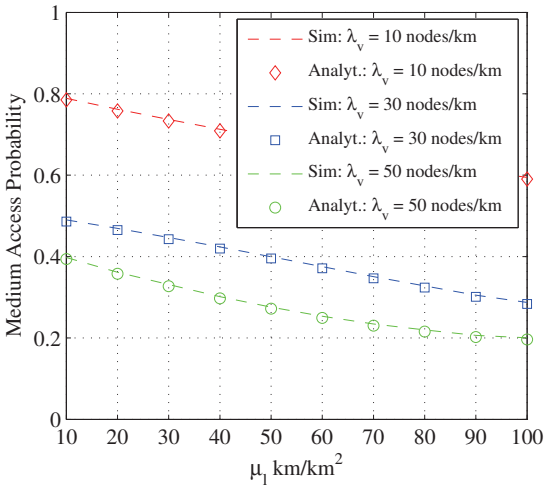


Fig. 5: Medium access probability (MAP) versus road density $\mu_l$

well as the variation of the road density, and show the results in Figures 4 and 5, respectively. Figure 4 displays the MAP for a fixed road density while varying the DSRC node density when voice traffic is transmitted. In particular, the analytical MAP and the MAP obtained from Monte Carlo simulations are plotted as the node density increases from 10 to 100 nodes$/$km for different road densities $\mu_l$. We observe that the analytical MAP in (2) provides an accurate fit to the simulation results for the different DSRC node densities. In addition, Figure 4 shows that the highest MAP achieved is naturally when we have the smallest $\lambda_v$, where MAP is equal to 0.79 for $\lambda_v = 10$ nodes$/$km. Moreover, as the DSRC node density $\lambda_v$ increases from 10 to 100 nodes/km, the MAP decreases rapidly to 0.2 when $\lambda_v = 100$ nodes/km. This can be explained by the fact that as the node density increases per road, the number of nodes in the sensing range of a particular node will increase. Hence, more nodes will contend to access the channel and this will naturally lead to a decrease in the MAP per node. We note here that although such a relationship is expected, the plot reveals the extent to which the MAP is impacted as the density increases. Furthermore, we can see that as the density of roads $\mu_l$ increases from 10 to 50 km$/$km$^2$, the MAP of a DSRC node experiences a further decrease of around 12 % on average. On the other hand, Figure 5 shows the MAP for a fixed DSRC node density where the analytical MAP and the MAP obtained from Monte Carlo simulations are plotted as the road density increases from 10 to 100 km$/$km$^2$. Similarly, Figure 5 shows that the analytical MAP in (2) provides an accurate fit to the simulation points for different road densities. Also, we can observe that the highest MAP achieved is when we have the smallest road density $\mu_l$ where MAP is equal to 0.79 for $\mu_l = 10$ km/km$^2$. However, as the road density $\mu_l$ increases from 10 to 100 km/km$^2$, the MAP decreases slowly and linearly to 0.59 when $\mu_l = 100$ km/km$^2$. Naturally, as we increase the density of roads $\mu_l$, the number of contending nodes increases proportionally but slowly, thus making its effect minimal as compared to the increase of the density of nodes per road $\lambda_v$. Furthermore, we can see that as the density of nodes $\lambda_v$ increases from 10 to 50 nodes$/$km, the MAP of a DSRC node experiences a further decrease: around 35 % on average at $\lambda_v = 30$ nodes$/$km, and 55% on average at $\lambda_v = 50$ nodes$/$km.

Finally, we present in Figures 6 and 7, the MAP for DSRC nodes carrying voice and background traffic, where we consider 50% voice traffic and 50% background traffic. Figure 6 presents the effect of increasing the DSRC node density $\lambda_v$ on the MAP of DSRC nodes where we can see that the MAP of DSRC nodes carrying voice traffic is higher than that of nodes carrying background traffic. This is due to the fact that DSRC nodes transmitting voice traffic use a smaller contention window (CW) size than the one used for background traffic. A similar trend is seen in Figure 7 as we increase the road density $\mu_l$. However, the MAP of both voice and background traffic decreases more with the increase in the road density

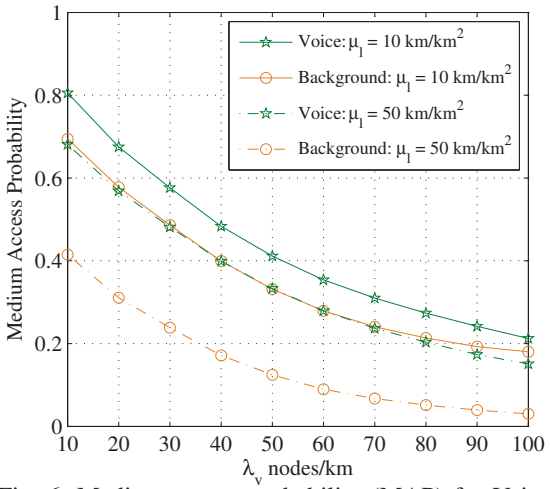


Fig. 6: Medium access probability (MAP) for Voice and Background Traffic ($\mu_l = 35\,\mathrm{km/km^2}$)

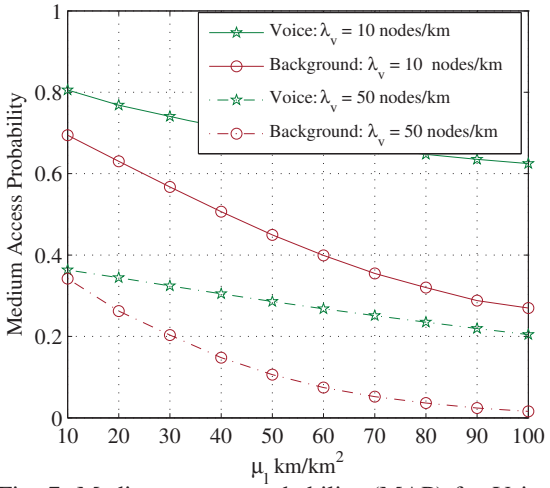


Fig. 7: Medium access probability (MAP) for Voice and Background Traffic ($\lambda_v = 20\,\mathrm{nodes/km}$)

$\mu_l$. Also, we can see that the MAP of nodes with voice traffic remains away from zero as either $\lambda_v$ or $\mu_l$ increases, whereas the MAP of nodes with background traffic decays fast with the increase of $\lambda_v$ or $\mu_l$.

## V. Conclusions

We have presented a framework based on stochastic geometry for analyzing the medium access probability in a DSRC network. Instead of assuming a fixed medium access probability (MAP) of nodes. We base our model on the IEEE 802.11p standard where we derive the MAP of DSRC nodes in a vehicular network composed of wireless nodes that are located on a system of roads. We model the roads using a Poisson line process (PLP) and the locations of nodes on each road as a homogeneous 1D Poisson point process (PPP). The presented model considers the effect of interference as well as the carrier sense multiple access with collision avoidance (CSMA/CA). We validated the analytical model against Monte Carlo simulations, and showed a close agreement between the MAP obtained from the model and from the simulations. Moreover, we illustrated the sensitivity of the MAP to the variations in the node and road densities. The proposed MAP model represents a useful tool that could be used in the design of future DSRC network deployments.

## Acknowledgments

The authors would like to acknowledge the support of Issam and Mohamad Darwish fund.

## References

[1] G. Karagiannis et al., “Vehicular Networking: A Survey and Tutorial on Requirements, Architectures, Challenges, Standards and Solutions," in IEEE Communications Surveys & Tutorials, vol. 13, no. 4, pp. 584-616, Fourth Quarter 2011.

[2] F. Martinez et al., “Emergency services in future intelligent transportation systems based on vehicular communication networks,” IEEE Trans. Intell. Transp. Syst. Mag., vol. 2, no. 2, pp. 6âĂŞ20, Oct. 2010.

[3] Part 11: Wireless LAN Medium Access Control (MAC) and Physical Layer (PHY) Specifications Amendment 6: Wireless Access in Vehicular Environments. IEEE std 802.11p-2010, pages 1-51. July 2010.

[4] J. Liu, G. Naik, J.M. Park,“Coexistence of DSRC and Wi-Fi: Impact on the Performance of Vehicular Safety Applications”, 2017 *IEEE* International Conference on Communications (ICC), Paris, 2017, pp. 1-6.

[5] *IEEE* Std 802.11-2012, *IEEE* standard for information technology telecommunications and information exchange between systems local and metropolitan area networks specific requirements part 11: Wireless lan MAC and PHY.

[6] S. N. Chiu, D. Stoyan, W. S. Kendall, and J. Mecke. Stochastic geometry and its applications. John Wiley & Sons, 2013.

[7] M. Haenggi. Stochastic geometry for wireless networks. Cambridge University Press, 2012.

[8] B. BĂĆaszczyszyn, M. Haenggi, P. Keeler, and S. Mukherjee. Stochastic geometry analysis of cellular networks. Cambridge University Press, 2018.

[9] H. Q. Nguyen, F. Baccelli and D. Kofman, “A stochastic geometry analysis of dense IEEE 802.11 networks”, in *IEEE INFOCOM*, pp. 1199-1207, May 2007.

[10] J. G. Andrews, F. Baccelli, and R. K. Ganti. A tractable approach to coverage and rate in cellular networks. IEEE Transactions on Communications, 59(11):3122âĂŞ3134, November 2011.

[11] Y. Li, F. Baccelli, J. G. Andrews et al., “Modeling and Analyzing the Coexistence of Wi-Fi and LTE in Unlicensed Spectrum," *IEEE Trans. Wireless Commun.*, vol. 15, no. 9, pp. 6310-6326, Sept. 2016.

[12] A. k. Ajami and H. Artail, “On The Modeling and Analysis of Uplink and Downlink IEEE 802.11ax Wi-Fi With LTE in Unlicensed Spectrum," *IEEE Trans. Wireless Commun.*, vol. 16, no. 9, pp. 5779-5795, Sept. 2017.

[13] A. k. Ajami and H. Artail,“Fairness in future Licensed Assisted Access (LAA) LTE networks: What happens when operators have different channel access priorities?," in *2017 IEEE Int. Conf. Commun. (ICC)*, Paris, France, 2017, pp. 67-72.

[14] Michigan Department of transportation (MDoT) and the Center for Automotive Research (CAR). Connected Vehicle Technology Industry Delphi Study. Sep. 2012.

[15] Q. Cui, N. Wang, and M. Haenggi, “Spatial point process modeling of vehicles in large and small cities”, in 2017 IEEE Global Communications Conference, pages 1âĂŞ7, Dec 2017.

[16] C.S. Choi and F. Baccelli. Poisson cox point processes for vehicular networks. arXiv preprint arXiv:1801.04556, 2018.

[17] A. Ajami and H. Artail, “Analyzing the Impact of the Coexistence With IEEE 802.11ax Wi-Fi on the Performance of DSRC Using Stochastic Geometry Modeling," in *IEEE Transactions on Communications*, vol. 67, no. 9, pp. 6343-6359, Sept. 2019.

[18] V. V. C. Ravi and H. S. Dhillon, “Coverage Analysis of a Vehicular Network Modeled as Cox Process Driven by Poisson Line Process,” *IEEE Trans. Wireless Communications*, vol. 17, no. 7, pp. 4401–4416, 2018.

[19] Goldsmith, A. (2005). Wireless Communications. Cambridge: Cambridge University Press. doi:10.1017/CBO9780511841224